ASSESSING THE DRIVERS CONTROLLING THE DEVELOPMENT OF AIRBORNE LAYERS IN POWDER SNOW AVALANCHES THROUGH INFRASOUND ANALYSIS

Betty Sovilla[1,*], Cristina Pérez-Guillén[1], Anselm Köhler[2], Emanuele Marchetti[3], Emma Suriñach[4]

[1] WSL Institute for Snow and Avalanche Research SLF , Davos, Switzerland
[2] Department for Natural Hazards, Austrian Research Centre for Forests, Innsbruck, Austria
[3] Department of Earth Sciences, University of Firenze, Firenze, Italy
[4] RISKNAT Avalanches Research Group, Geomodels and Earth Sciences Faculty, University of Barcelona, Barcelona, Spain

ABSTRACT: Powder snow avalanches (PSAs) with high-energy airborne layers pose a significant threat to buildings and facilities intended to be protected by infrastructure like dams. However, understanding the factors driving the development of these hazardous suspension layers remains challenging due to limited experimental data and understanding of PSA generation mechanisms. Recent advances in infrasound research have revealed that infrasound is primarily generated from particle clusters suspended in the airborne layer of PSAs by turbulent eddies or ejected from the denser basal layer. In addition, the infrasound signal is correlated with the kinetic energy of all active particles within these layers, offering a promising avenue to address this challenge. In this study, we analyze 27 infrasound signals collected at the Vallée de la Sionne test site in Switzerland, covering various PSA dimensions and degrees of powder cloud development. We systematically quantify amplitudes, cumulative intensities, and energy distribution extracted from the infrasound measurements. These findings are compared with reference data from a high-resolution GEODAR radar to assess the evolution of the powder cloud in both temporal and spatial dimensions. Subsequently, we correlate this information with boundary conditions such as snow cover, and previous avalanche activity to understand their influence on the development of high-energy airborne layers in PSAs. Conversely, we explore how these factors contribute to the decay of the powder cloud, thereby enhancing our ability to assess and mitigate avalanche hazard.

Keywords: Powder Snow Avalanches, Infrasound, Turbulent Particle-Laden Flow, Turbulent Multiphase Flow

1. INTRODUCTION

Powder snow avalanches (PSAs) have the potential to transport large quantities of material through their airborne layers, posing a significant threat to protected areas with critical infrastructure, such as dams. Despite this threat, the dynamics and energy of these suspension layers are not well understood, presenting a major challenge to effectively assess and mitigate associated hazards.
Particles suspended within a PSA are organized into clusters, which can have densities several times greater than that of the surrounding air (Sovilla et al., 2015). Recent studies have shown that these high-velocity, high-density particle clusters generate air pressure waves in the surrounding atmosphere (Sovilla et al., submitted). These pressure waves can be detected by infrasound sensors (Kogelnig et al., 2011; Marchetti et al., 2020), with the infrasound energy being proportional to the kinetic energy of the suspended material (Sovilla et al., submitted; Landau and Lifshitz, 1987). This makes infrasound measurements an indirect method for assessing the energy of the clusters in suspension, and thereby estimating the destructive potential of the airborne layer in PSAs.
Leveraging this new finding, we aim to analyze 27 infrasound signals from PSAs of varying dimensions collected at the Vallée de la Sionne test site in Switzerland (VdlS). The avalanches will be ranked based on the infrasound energy generated by their airborne layers, and the ten most energetic avalanches will be further examined to determine where most of the energy was developed and how the boundary conditions along the path contributed to this evolution.

2. METHODS

2.1 Infrasound measurements and signal processing

Infrasound has been measured in VdlS since 2008 using a Chaparral Model 24 sensor with a bandwidth of 0.1 Hz to 200 Hz (Kogelnig et al., 2011). The sensor is positioned on the valley bottom and captures signals from avalanches as they travel from the release point, up to 2.5 km away, to the deposit area (Fig. 1). Throughout the winter season, infrasound data is collected at 100 Hz, in both continuous and trigger modes.
The infrasound data $A(t)$ is bandpass filtered from 0.1 to 50 Hz (Fig 2a, green line), and then further processed by calculating its root mean square (RMS) envelope $A_{RMS}(t)$ defined as:

*Corresponding author address:
Betty Sovilla, WSL Institute for Snow and Avalanche Research SLF
7260 Davos Dorf, Switzerland;
tel: +41 81 4170 263; email: sovilla@slf.ch

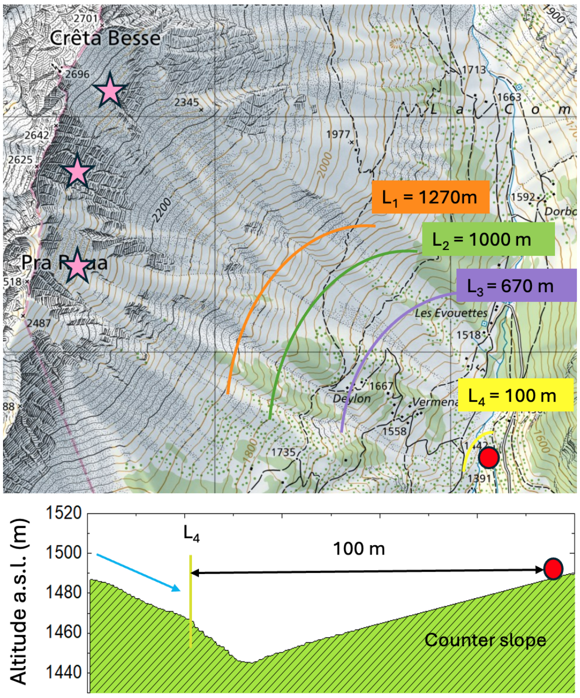

Figure 1: Overview map of the VdlS test site (upper panel). The pink stars highlight the positions of the main release areas, while the red dot marks the location of the infrasound sensor and the GEODAR. Colored lines represent the reference locations. The lower panel shows a sketch of the topography at the bottom of the slope, near the infrasound sensor. A counterslope in this area abruptly halts avalanches, potentially causing the release of high-energy peaks in the infrasound signal. The blue arrow indicates the direction of the incoming avalanche.

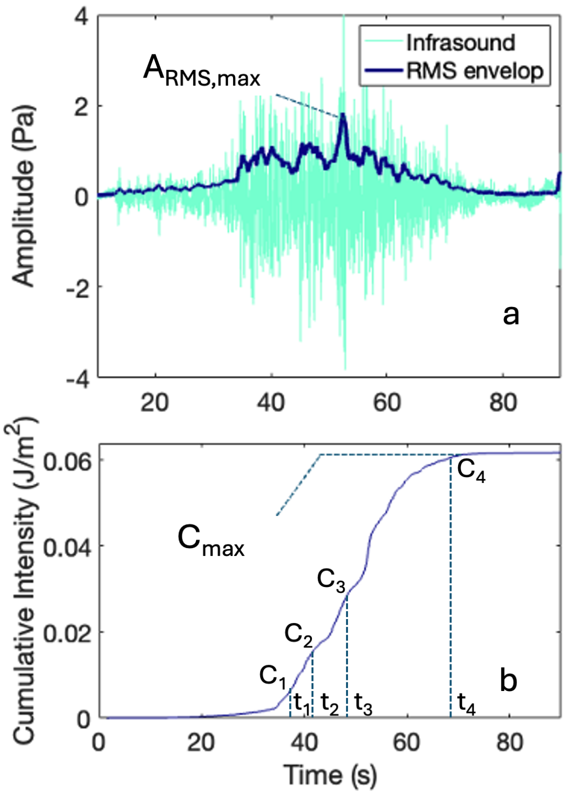

Figure 2: (a) Infrasound signal of avalanche #20150020 with its RMS envelope. (b) Cumulative intensity calculated from the RMS envelope.

$$A_{RMS}(t) = \sqrt{\frac{1}{T}\int_{t-T}^{t} A(\tau)^2 \, d\tau} \tag{1}$$

where $T = 2$ s is the integration time window (Fig 2a, blue line).

The infrasound intensity at the receiver I_R [W/m^2], can then be calculated using the equation:

$$I_R(t) = \frac{A_{RMS}(t)^2}{\rho c} \tag{2}$$

where ρ [kg/m^3] is the air density and c [m/s] is the speed of sound.

Finally, the infrasound energy at the receiver is derived as cumulative function $C(t)$ [J/m^2] of the infrasound intensity (Fig 2b):

$$C(t) = \int_0^t I_R(\tau) \, d\tau. \tag{3}$$

By leveraging recent findings that show infrasound energy is proportional to the kinetic energy of particle clusters in suspension (Sovilla et al., submitted), we will use the cumulative function $C(t)$ as a proxy for the energy of the mass in suspension in our avalanches. While this approach does not provide the absolute value of the kinetic energy, it allows us to compare and rank avalanches by their energy levels, helping us identify which avalanches have developed powerful suspensions and which have not.

2.2 Reference measurements

The GEODAR radar (Köhler et al., 2018b) is installed close to the infrasound sensors, inside a reinforced building (red dot in Fig. 1). The radar and infrasound measurements are time synchronized, enabling the linking of infrasound data to the avalanche position in time and space, information that can be easily extracted from the radar data. Specifically, GEODAR measurements are used to assess the time when the avalanche front reaches particular locations along the avalanche paths (Fig. 3). Each location is identified by its line-of-sight distance from the radar and infrasound sensor.

Reference locations are chosen as follows:

- L_1: Inside a channelized area, 1270 m from the instruments
- L_2: At the exit of the channelized area, 1000 m from the instruments
- L_3: At the location of a 20 m tall pylon located in the open slope in the runout area, 670 m from the instruments

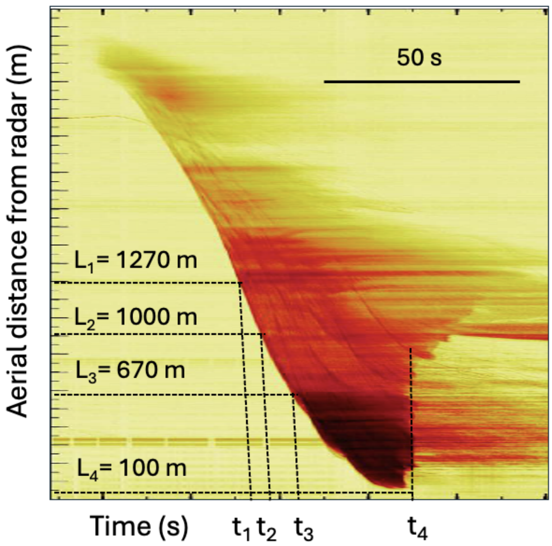

Figure 3: GEODAR radar MTI plot of avalanche #20150020. The reference locations L_1 to L_4 are indicated. Infrasound arrival times t_1 to t_4 have been corrected for acoustic propagation.

- L_4: Before the avalanche impacts against a counter slope, 100 m from the instruments

The times t_1 to t_4 when the avalanche reaches these locations are then used to extract the corresponding cumulative intensity C_1 to C_4 (Eq. 3) at these specific points, as indicated in Fig. 2b.

2.3 Snow depth parametrization

The infrasound measurements are subsequently correlated with the snow cover conditions within the avalanche path. Snow conditions are monitored by two weather stations. Data are collected from the Donin du Jour meteorological station, situated at 2385 m a.s.l., which is representative of the release conditions (top station), and from a second station installed at 1690 m a.s.l., which characterizes the snow conditions at the onset of the runout zone (bottom station).

Assuming that both the total snow depth (h_s) and the new snow depth over the last 72 hours (h_{N72}) are relevant for the development of the PSA airborne layers, we propose a snow cover parametrization S that integrates these factors. The parameter S is defined as the sum of two normalized contributions:

$$S = \left(\frac{h_{N72,\text{top}} + h_{N72,\text{bottom}}}{H_{N72,\text{top}} + H_{N72,\text{bottom}}} \right) + \left(\frac{h_{s,\text{top}} + h_{s,\text{bottom}}}{H_{s,\text{top}} + H_{s,\text{bottom}}} \right) \quad (4)$$

In this formula, the first term represents the sum of the new snow depth over 72 hours at both the top and bottom stations, normalized by the maximum values $H_{N72,\text{top}}$ and $H_{N72,\text{bottom}}$ observed across all avalanches. This normalization ensures that the contribution is dimensionless and scaled between 0 and 1.

The second term similarly represents the normalized sum of the total snow depth at the top and bottom stations, using the maximum values $H_{s,\text{top}}$ and $H_{s,\text{bottom}}$ for normalization. By adding these two terms, S provides a composite measure of the snow cover depth, accounting for both recent snowfall and the total snowpack depth in the release and deposition areas.

3. DATA

In our analysis, we utilized 27 infrasound measurements of PSAs collected at VdlS. The data were processed according to the Eqs. 1 and 3, and the maximum RMS amplitudes, $A_{RMS,max}$, and cumulative intensity, C_{max}, for each avalanche, are plotted in Fig. 4. Since infrasound sensors record air pressure fluctuations generated by material in suspension (Sovilla et al., submitted), and these fluctuations are proportional to the kinetic energy of the material, this representation allows us to rank avalanches based on the energy of the suspended material. It is evident that, although all these avalanches developed a significant airborne component, the energy content of this layer varied greatly between them.

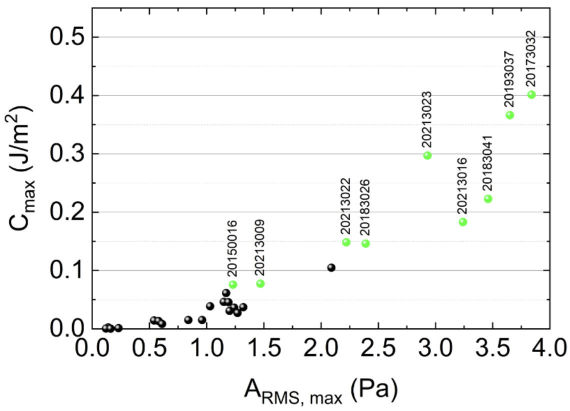

Figure 4: The maximum infrasound RMS amplitude, $A_{RMS,max}$, is plotted against the maximum cumulative intensity, C_{max}, for all analyzed avalanches. This representation shows that the infrasound signals encompass a wide range of avalanches, characterized by varying degrees of development and energetic content in the airborne layers. Avalanches identified by a reference number and a green dot will be further analyzed in this study.

4. RESULTS AND DISCUSSION

4.1 PSA Development by Location

To understand the conditions that favor the development of high-energy suspension layers in PSAs, we further analyzed the avalanches shown in Fig. 4 that exhibited the highest cumulative intensity. For each avalanche, we calculated the rate of change in cumulative intensity, $R(t_i)$, between specific locations

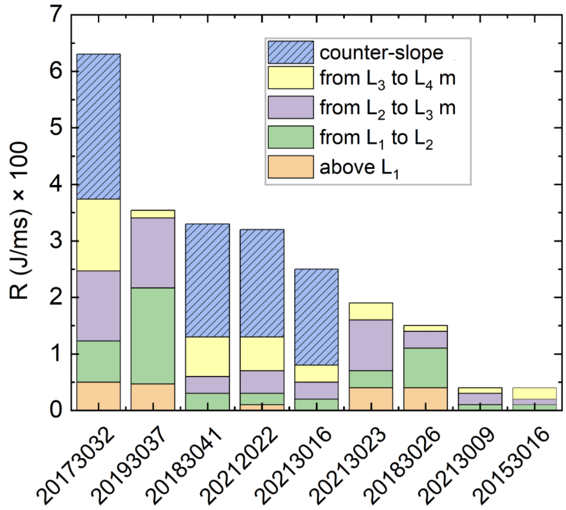

Figure 5: The rate of change in cumulative intensity per unit time between consecutive locations L_{i-1} and L_i, $R(t_i)$, is plotted for the most energetic avalanches in our dataset. Each color represents a specific section of the path. Avalanches that reach the counterslope with very high energy generate abrupt rapid pressure disturbances, which are indicated in the graph by a pastel blue hatched area.

L_i along the path, as defined in section 2.2, where t_i corresponds to the time at location L_i. The rate of change in cumulative intensity is given by:

$$R(t_i) = \frac{C(t_i) - C(t_{i-1})}{t_i - t_{i-1}} \quad \text{for } i = 1, 2, 3, 4 \qquad (5)$$

This normalization is crucial because slower avalanches may show larger cumulative intensity values simply due to their longer duration. By normalizing the change in cumulative intensity with respect to time, we obtain a more accurate measure of intensity changes that accounts for differences in avalanche speed.

The $R(t_i)$ values are plotted in Fig. 5 for the most energetic avalanches in our dataset. Avalanches that reach the counter slope at the bottom of the valley (Fig. 1, lower panel), with particularly high energy, can generate abrupt rapid pressure disturbances (Fig. 6). This phenomenon results in a sharp increase in cumulative intensity. The rate of change in cumulative intensity for this effect is also depicted in Fig. 5.

It is important to note that $R(t_i)$ is not corrected for acoustic dissipation. Consequently, the intensity rates at more distant locations are underestimated compared to those at nearby locations.

Figure 5 shows that while all of these avalanches developed an important airborne component, only four reached the counter slope with considerable force, as indicated by the formation of abrupt rapid pressure disturbances. Among these, avalanche #20173032 experienced optimal conditions from release to deposition, resulting in high-energy air-

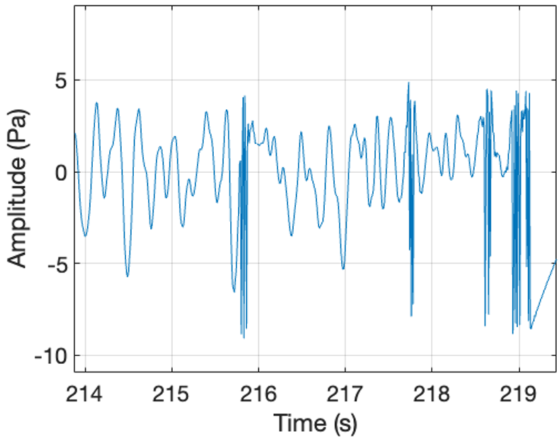

Figure 6: Detail of the infrasound signal generated by the avalanche #20213022 on the counter slope showing sudden and pronounced fluctuations, indicating abrupt rapid pressure disturbances. These disturbances typically have a brief duration, representing single, sharp pulses of energy.

borne layers throughout the entire avalanche path.

Interestingly, three of the four avalanches that reached the bottom of the valley with high momentum only developed their high-energy suspension in the lower part of the track (L_3 to L_4). Conversely, avalanche #20193037, despite being initially promising until L_3, completely decayed below the pylon.

These data suggest that conditions in the upper part of the track are not the sole determinants of whether an avalanche will retain its energy through to the counter slope. Instead, local conditions in the runout zone play a crucial role in determining the final impact of the avalanche.

4.2 PSAs Development and Snowcover

The development of highly energetic and long-runout PSAs is typically associated with major snowstorms, which lead to substantial new snow accumulations. As a result, the amount of new snow is often considered the most significant meteorological variable linked to dry-snow avalanche formation, with threshold values for new snow measured at nearby weather stations commonly used as an indicator of hazard potential (Schweizer et al., 2009).

Our preliminary results, shown in Fig. 5, suggest that also snow conditions near the counter slope may be particularly crucial in determining whether an avalanche can maintain a high-energy airborne layer through to final deposition.

In this context, our snow cover parameterization, S (Eq. 4), not only considers new snow depth at the altitude of the release area but also incorporates new snow depth at the location of the runout. Furthermore, since large avalanches typically entrain much of the available snow along their path, potentially promoting long runout distances (Sovilla et al., 2006), we also account for total snow depth in both the release and deposit areas.

Figure 6 illustrates that the newly defined snow parameter, S, correlates well with the overall energy of the airborne layers (green-marked avalanches) for the largest measured avalanches. However, the same figure also shows that several PSAs developed an airborne component, but their sizes were smaller than expected given the large amount of erodible snow on the ground (black dots). Moreover, this parameterisation does not effectively predict which avalanches will actually reach the counter slope with high energy. For instance, avalanche #20193037, which had the second-largest snow parameter value, failed to produce abrupt rapid pressure disturbances at the counter slope. Consequently, a simple snow depth parametrization, while qualitatively useful to identify potential danger, would have resulted in many false alarms (Schweizer et al., 2009).

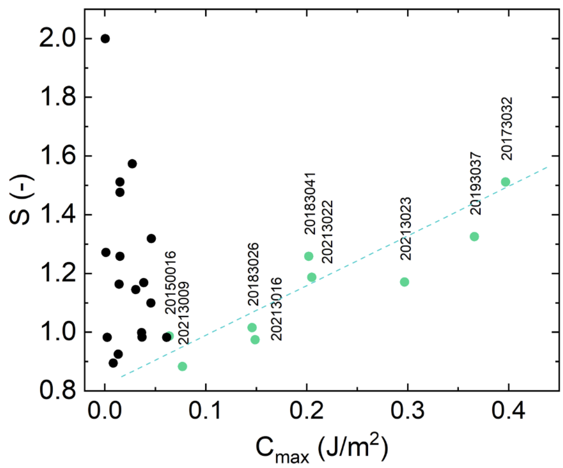

Figure 7: The snow parameter, S, is plotted against the maximum cumulative intensity, C_{max}, for all analyzed avalanches. Green dots highlight the avalanches analysed in Fig. 5. For these avalanches, the maximum cumulative intensity, representing a proxy for the energy of the material in suspension, correlates with snow height and new snow accumulation along the path. The green dashed line serves as a visual guide.

4.3 Other Factors in PSA Development

Thus, in addition to snow depths, there are other critical factors that must be considered to better predict the evolution of the airborne layers. For instance, we attribute the decay of the airborne layers in the runout area of avalanche #20193037 to a combination of high air temperatures and an unfavorable basal sliding surface. Although the air temperature at the release point was around -2.5 °C, which favored the development of a high-energy airborne layer, the temperature in the deposition area rose to 4.5 °C. This higher air temperature, mixing with the turbulent layer, likely contributed to the melting of a significant portion of the suspended particles (Fischer et al., 2018). Furthermore, the avalanche entrained very warm snow down to the ground, which reduced the mobility of the basal dense layer and probably influenced the development of the avalanche (Köhler et al., 2018a).

In contrast, avalanches #20213016, #20183041, and #20212022, which descended after an intense avalanche season, benefited from large amounts of snow deposited in the runout zone by previous avalanches. In the runout zone, the air temperature remained below the melting point and the sliding surface was smooth and cold due to these old deposits. This combination of factors supported the continued development of the powder cloud, enhancing the avalanches' overall energy and reach.

Finally, the avalanches that failed to develop energetic airborne layers, as indicated by the black dots in Fig. 6, can often be attributed to conditions in the release and flow zones. Typically, in these cases, the release area did not reach the critical size necessary to counterbalance the energy lost through the entrainment of the deep snow cover. This resulted in avalanches that were unable to fully develop a sustained dynamic (Ligneau et al., submitted). Furthermore, in many cases, these avalanches could not become powerful simply because the snow measurements from nearby weather stations did not accurately reflect the conditions within the avalanche path, as portions of the snow cover had already been removed by previous avalanche activity.

5. CONCLUSION

Infrasound measurements provide a powerful tool for studying the development of the airborne layer in PSAs. For instance, we show that combining infrasound data with actual conditions inside the avalanche basin allows us to pinpoint the key factors driving the formation of powerful and potentially dangerous PSAs. Our findings highlight the significant roles of new snow depth and total snow depth in the release and runout zones, along with critical factors like snow and air temperature and the condition of the sliding surface, particularly near infrastructure.

Infrasound also provides crucial insights into the energy dynamics within the avalanche cloud, allowing us to rank avalanches based on the energy they generate. This capability is invaluable for the real-time detection and assessment of avalanche dimensions according to flow regime. Furthermore, when combined with seismic sensors, infrasound may enhance our ability to accurately partition energy between airborne and dense layers (Marchetti et al., 2020). Improved energy partitioning is essential for better predicting and monitoring the reach and impact of avalanches, ultimately leading to more effective hazard assessment and enhanced safety measures in vulnerable areas .

ACKNOWLEDGEMENT

The GEODAR data were acquired as part of the Swiss National Science Foundation grants No. 169640, as well as support from the canton of Valais. The infrasound data were obtained through the CGL2017-84720-R project of the University of Barcelona, funded by the Spanish Ministry MINEICO-FEDER. We express gratitude to the UB Avalanche Team, particularly Pere Roig-Lafon, for their assistance in acquiring the infrasound data. Special acknowledgment is extended to our colleagues at the electronics and workshop of SLF for their invaluable support.

References

Fischer, J.-T., Kaitna, R., Heil, K., and Reiweger, I.: The Heat of the Flow: Thermal Equilibrium in Gravitational Mass Flows, Geophysical Research Letters, 45, 11,219–11,226, doi:10.1029/2018GL079585, 2018.

Kogelnig, A., Suriñach, E., Vilajosana, I., Hübl, J., Sovilla, B., Hiller, M., and Dufour, F.: On the complementariness of infrasound and seismic sensors for monitoring snow avalanches, Natural Hazards and Earth System Sciences, 11, 2355–2370, doi:10.5194/nhess-11-2355-2011, 2011.

Köhler, A., Fischer, J.-T., Scandroglio, R., Bavay, M., McElwaine, J., and Sovilla, B.: Cold-to-warm flow regime transition in snow avalanches, The Cryosphere, 12, 3759–3774, doi:10.5194/tc-12-3759-2018, 2018a.

Köhler, A., McElwaine, J. N., and Sovilla, B.: GEODAR Data and the Flow Regimes of Snow Avalanches, Journal of Geophysical Research: Earth Surface, 123, 1272–1294, doi:10.1002/2017JF004375, 2018b.

Landau, L. D. and Lifshitz, E. M.: Fluid Mechanics, Second Edition: Volume 6 (Course of Theoretical Physics), Course of theoretical physics / by L. D. Landau and E. M. Lifshitz, Vol. 6, Butterworth-Heinemann, 2 edn., 1987.

Ligneau, C., Sovilla, B., and Gaume, J.: Mobility of cohesive granular flows over erodible beds: insights from discrete element simulations, Granular Matter, submitted.

Marchetti, E., van Herwijnen, A., Christen, M., Silengo, M. C., and Barfucci, G.: Seismo-acoustic energy partitioning of a powder snow avalanche, Earth Surface Dynamics, 8, 399–411, doi:10.5194/esurf-8-399-2020, 2020.

Schweizer, J., Mitterer, C., and Stoffel, L.: On forecasting large and infrequent snow avalanches, Cold Regions Science and Technology, 59, 234–241, doi:10.1016/j.coldregions.2009.01.006, 2009.

Sovilla, B., Burlando, P., and Bartelt, P.: Field experiments and numerical modeling of mass entrainment in snow avalanches, Journal of Geophysical Research: Earth Surface, 111, doi:10.1029/2005JF000391, 2006.

Sovilla, B., McElwaine, J. N., and Louge, M. Y.: The structure of powder snow avalanches, Comptes Rendus Physique, 16, 97–104, doi:10.1016/j.crhy.2014.11.005, 2015.

Sovilla, B., Marchetti, E., Kyburz, M. L., Köhler, A., Huguenin, P., Calic, I., Kohler, M. J., Suriñach, E., and Pérez-Guillén, C.: The dominant source mechanism of infrasound generation in powder snow avalanches, Geophysical Research Letters, submitted.